

Theory of Correlated Insulator(s) and Superconductor at $\nu = 1$ in Twisted WSe₂

Sunghoon Kim,* Juan Felipe Mendez-Valderrama,* Xuepeng Wang,* and Debanjan Chowdhury†
Department of Physics, Cornell University, Ithaca, New York 14853, USA.

The observation of a superconducting phase, an intertwined insulating phase, and a continuous transition between the two at a commensurate filling of $\nu = 1$ in bilayers of twisted WSe₂ (tWSe₂) at $\theta = 3.65^\circ$ raises a number of intriguing questions about the origin of this phenomenology. Starting with a simplified three-orbital model of tWSe₂, including an on-site and nearest-neighbor density-density interactions, as well as a chiral-exchange interaction, we discuss the possibility of a displacement-field induced direct superconductor to quantum spin-liquid Mott insulator transition at $\nu = 1$ using parton mean-field theory. We discuss the nature of these correlated insulators, their expected evolution with the displacement-field, and their phenomenological properties. Further experiments will likely help unravel the mysteries tied to this fascinating experimental platform.

Introduction.- Superconductivity (SC) in two-dimensional (2D) electronic materials at low carrier densities has captivated the attention of physicists in recent years. The observation of SC in moiré [1–5] as well as moiré-less graphene [6–9] in the vicinity of correlation-induced insulators [10] and spontaneously spin (or valley) polarized metallic states [11] has raised the question of the extent to which pairing is due to the “proximate” electronic orders. The role of electron-electron vs. electron-phonon interactions in inducing SC in these platforms has also been scrutinized intensely, even as the experimental situation remains largely unclear [12–14]. The recent discovery of superconductivity and an intertwined correlated insulator in twisted bilayers of WSe₂ (tWSe₂) near $\theta = 3.65^\circ$ only at a commensurate filling [15] present a number of fascinating puzzles that requires a critical examination of strong-coupling effects, originating from electronic interactions.

While previous experimental work [16] argued for possible signatures of SC in a doped insulator in tWSe₂, the recent report [15] highlights a number of unconventional features tied to its origin. While SC is of course interesting in its own right, the associated phenomenology tied to the regime in the phase-diagram where SC appears makes the problem much more exciting from a theoretical perspective. We highlight below some of the important phenomenological observations which need to be taken into serious consideration from the outset, and which (in our opinion) point towards a strong-coupling perspective, beyond a purely fermiology-driven paradigm. First and foremost, the superconducting region occurs only in the vicinity of the commensurate filling $\nu = 1$, and away from the van-Hove filling. Second, the predominant phase at $\nu = 1$ is a correlated interaction-induced insulator, which only gives way to SC over a narrow range of displacement fields near $E = 0$ below T_c . Notably, both the insulating and superconducting phases appear in the “layer-hybridized” regime, as opposed to the “layer-polarized” regime. Third, there appears to be a displacement field-induced *continuous* and *direct* superconductor-insulator transition at $\nu = 1$. The insulator yields no topological response, in as far as electrical transport is concerned, and re-

veals fluctuating local-moments at high temperatures [17].

Superconductor-Insulator transition.- At first glance, the superconductor-insulator transition suggests the possibility of the insulator being a “failed-superconductor” [18] — a localized crystal of phase-incoherent (electronic) Cooper-pairs. However, once the Cooper-pairs develop phase-coherence, it is unclear why the superconducting phase only survives in the vicinity of $\nu = 1$, rather than a wider range of dopings [19]. Clearly, disorder can be an essential part of resolving this puzzle, but we turn to other alternative scenarios in this manuscript. Our interpretation of the experimental data suggests that the origin of pairing, or the “glue”, is potentially present in the insulator itself. In other words, it is not the pairing of electrons, but of other particles (e.g. spinons) in the “parent” insulating phase, that might be responsible for the subsidiary electronic pairing in the superconducting phase, separated from the parent insulator via a quantum phase transition. Our proposed scenario is distinct from a weak-coupling electron fermiology-driven instability [20–27] or a doping-induced instability [28–33], which is generically not expected to yield a direct continuous superconductor-insulator transition at a fixed commensurate filling.

Our basic proposal for the phenomenology at $\nu = 1$ is effectively of a fully gapped quantum spin liquid insulator [34, 35], where the electron fractionalizes into neutral fermionic spinons which are paired, and a gapped holon which carries the electronic charge. As noted above, the fermionic pairing is arising within the insulator itself and the transition into the electronic superconductor at a fixed filling arises once the holons condense as a function of the displacement-field [36]. Clearly, the doped quantum spin liquid can, in principle, harbor SC; however, we speculate at the end on why this tendency can be suppressed in the present setting. In this manuscript, starting from a model Hamiltonian that is believed to capture many of the essential microscopic details of the electronic bandstructure, topological character, and interactions, we will analyze the above scenario for the interplay between the insulator and superconductor at the commensurate filling $\nu = 1$. While at this early stage many experimental aspects of the phenomenology remain yet to be investigated, and the theoretical modeling is possibly rudimentary, the lessons of our analysis are fairly general and will hopefully motivate further work in both theory and experiment.

* These authors contributed equally to this work

† debanjanchowdhury@cornell.edu

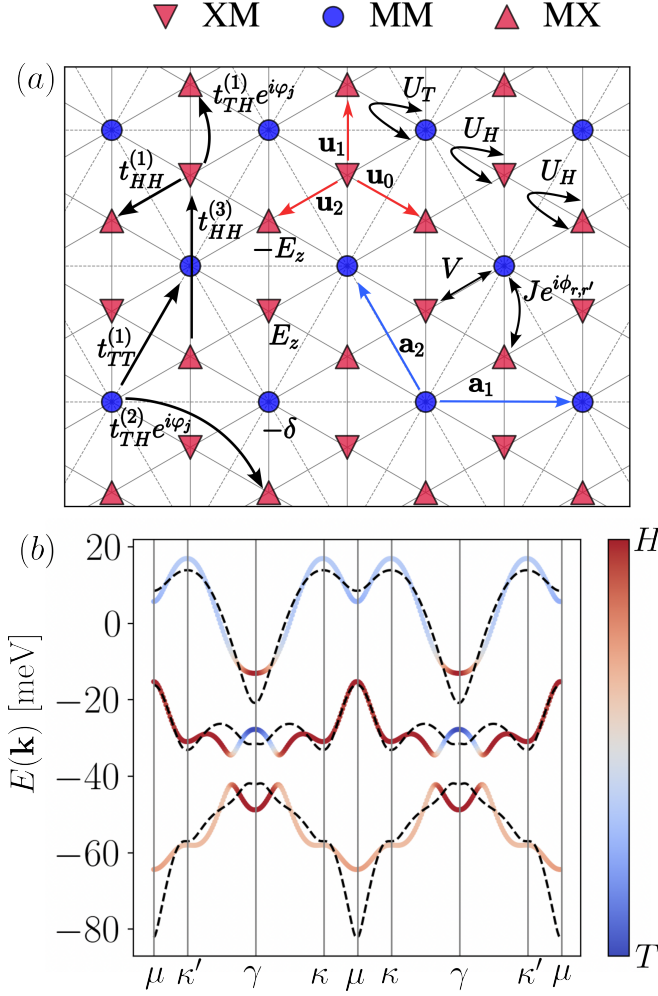


FIG. 1. (a) Schematic of the interacting three-orbital model for tWSe₂, where \bullet , \blacktriangledown , \blacktriangle symbols represent MM, XM and MX sites, respectively; see Eq. 1a and 3. (b) Non-interacting electronic dispersions of the continuum model (dashed lines) and the tight-binding fit to the three-orbital model (solid colored line), respectively, for the topmost, second, and third moiré valence bands. The color coding denotes honeycomb (H) for the MX/XM sites, and triangular (T) for the MM site.

Model.— To demonstrate the above scenario in a concrete setting, we start from a three-orbital electronic model [37] obtained from an underlying continuum model [38, 39]. The general features of the model derive from taking the quadratic approximation for the topmost valence band of the monolayer valley, K , which is spin-split due to the strong spin-orbit coupling [40]. The opposite valley is related by time-reversal symmetry (TRS) and for AA stacking, the bands from both layers will feature spin \uparrow (\downarrow) character for valley K ($-K$). The bands for the bottom and top layer are slightly displaced to the corners of the Brillouin zone κ_{\pm} , whose location is determined by the twist angle θ . For WSe₂, the interlayer tunneling and the moiré potential has been determined from large-scale DFT calculations [39]. At large twist angles, the two top-most bands in the continuum model feature equal valley contrast-

ing Chern numbers. Consequently, to capture the low energy physics of these bands, a minimal model including at least three orbitals is needed to achieve a local real space description [37, 41].

We focus on the following interacting model in what follows: $H = \sum_{\sigma=\uparrow,\downarrow} H_{\sigma} + H_{\text{int}}$,

$$H_{\uparrow} = \sum_{k,\tau} c_{k,\tau}^{\dagger} [h_{1,\tau}(\mathbf{k}) + h_{2,\tau}(\mathbf{k})] c_{k,\tau}, \quad \text{where} \quad (1a)$$

$$h_1(\mathbf{k}) = \begin{pmatrix} E_z - \mu & t_{TH}^{(1)} g_{\mathbf{k}} & t_{HH}^{(1)} f_{\mathbf{k}}^* \\ t_{TH}^{(1)} g_{\mathbf{k}}^* & -\delta - \mu & -t_{TH}^{(1)} g_{-\mathbf{k}} \\ t_{HH}^{(1)} f_{\mathbf{k}} & -t_{TH}^{(1)} g_{-\mathbf{k}} & -E_z - \mu \end{pmatrix}, \quad (1b)$$

$$h_2(\mathbf{k}) = \begin{pmatrix} 0 & -t_{TH}^{(2)} g_{-2\mathbf{k}} & t_{HH}^{(3)} f_{2\mathbf{k}} \\ -t_{TH}^{(2)} g_{-2\mathbf{k}}^* & t_{TT}^{(1)} h_{\mathbf{k}} & t_{TH}^{(2)} g_{2\mathbf{k}}^* \\ t_{HH}^{(1)} f_{\mathbf{k}} & t_{TH}^{(2)} g_{2\mathbf{k}} & 0 \end{pmatrix}. \quad (1c)$$

Here, $c_{k,\tau}$ represents a spinor in orbital space, and $h_1(\mathbf{k})$, $h_2(\mathbf{k})$ represent the nearest and further range hopping matrix elements, respectively. The displacement-field, E_z , modifies the on-site energies and μ is the chemical potential. At $E_z = 0$, the MX/XM sites are degenerate in energy, and split by an amount $\sim \delta$ relative to the energy of the MM sites. The hopping matrix-elements, t_{ab} ($a, b \equiv T, H$), for the triangular and honeycomb lattice sites are shown in Fig. 1(a). The associated momentum-space form-factors are defined as,

$$f_{\mathbf{k}} = \sum_{j=0,1,2} e^{i\mathbf{k}\cdot\mathbf{u}_j}, \quad g_{\mathbf{k}} = \sum_{j=0,1,2} e^{i2\pi(j-1)/3} e^{i\mathbf{k}\cdot\mathbf{u}_j}, \quad (2a)$$

$$h_{\mathbf{k}} = 2 \sum_{j=1,2,3} \cos(\mathbf{k} \cdot \mathbf{a}_j), \quad (2b)$$

where $\mathbf{a}_1 = (a_M, 0)$, $\mathbf{a}_j = C_3^{j-1} \mathbf{a}_1$, $\mathbf{u}_0 = (\mathbf{a}_1 - \mathbf{a}_2)/3$, $\mathbf{u}_j = C_3^j \mathbf{u}_0$, and a_M is the moiré lattice constant. The specific orbital content is that of orbitals localized at the XM/MX (H) and MM (T) stacking regions of the bilayer with an s -wave character. The former (H) are layer polarized as interlayer tunneling vanishes at these stacking regions, while the latter (T) is layer hybridized since MM stacking regions map to themselves under C_{2y} symmetry, implying that they possess mixed character from both layers [37].

It is useful to comment briefly on the tight-binding parametrization of the continuum model bandstructures. The careful choice of hoppings in the model is able to broadly capture the band topology of twisted TMD homobilayers by reproducing the C_3 eigenvalues of orbitals obtained from the continuum model at γ, κ , and κ' , which can be done by retaining nearest neighbour hoppings in $h_1(\mathbf{k})$ and is consistent with DFT [37, 39]. By additionally including further neighbour hoppings, the energetics of the topmost band can be reproduced to a high degree of accuracy at small twist angles. However, for $\theta = 3.65^\circ$, the top three bands of the continuum model for twisted WSe₂ feature a combination of topological indices that disallows a local description [42], which is reflected in the error incurred in the fit to the three orbital model in Fig. 1. Nevertheless, the uncertainties in the parameters of the continuum model, which neglects effects of lattice relaxation that can affect the topology and energetics of the remote

bands, leads us to focus on capturing only the topology of the two topmost bands. Phenomenologically, this allows us to study the low-energy physics of the experiment within a local description, but setting up the problem directly in momentum-space remains an interesting future direction. Even with this approximation, the Berry curvature distribution and quantum geometry of the topmost two bands can be reproduced faithfully from the continuum model. The integral of the Fubini-Study metric shows a particularly weak dependence on displacement field suggesting that localization of the Wannier orbitals at the level of the non-interacting bands is playing a subsidiary role and the main effect of the displacement field may be to introduce a sublattice potential difference between XM and MX stacking regions.

Turning now to the interactions,

$$H_{\text{int}} = U_H \sum_{r \in H} n_{r\uparrow} n_{r\downarrow} + U_T \sum_{r \in T} n_{r\uparrow} n_{r\downarrow} + V \sum_{r \in T, r' \in H} n_r n_{r'} + J \sum_{r \in T, r' \in H} \left[e^{i\phi_{r,r'}} c_{r\uparrow}^\dagger c_{r'\downarrow}^\dagger c_{r'\downarrow} c_{r\uparrow} + \text{h.c.} \right], \quad (3)$$

we have included an on-site repulsion U_H , U_T on the honeycomb and triangular sites, respectively, in addition to a nearest-neighbor (represented by \sum') repulsion, V . Finally, the chiral-exchange interaction, J , arises between the T and H sites directly by projecting the Coulomb-interactions to the relevant bands, and the phase-factors $\phi_{r,r'} = 2\pi n/3$ with n an integer that increases counter-clockwise labeling the six nearest neighbours around a T site. This term preserves the time-reversal symmetry as it can be rewritten as the weighted sum of a Heisenberg and a two-spin Dzyaloshinskii-Moriya interaction. Note that we have not included a super-exchange interaction across the two valleys in the above description since it is expected to be small; nevertheless, such an interaction will also drive the same pairing tendency of spinons [43].

Parton mean-field theory.- The parton representation proceeds in the usual fashion, where we express $c_{r,\ell,\sigma} = b_r f_{r,\ell,\sigma}$, where the b_r represent the spinless charged holon fields at site r , and the $f_{r,\ell,\sigma}$ denote spinful neutral spinons that also carry the orbital index ℓ . The local constraint that helps project the problem back to the physical Hilbert space is given by $\langle n_r^b \rangle + \langle \sum_{\ell,\sigma} n_{r,\ell,\sigma}^f \rangle = 1$. We begin by incorporating the mean-field decomposition of the above Hamiltonian, where the effect of the U , V - terms associated with the on-site and nearest-neighbor repulsions at the commensurate filling are included in the bosonic sector, and the effect of the chiral-exchange J - term is included in the fermionic sector, respectively. As a result, the ‘‘Mottness’’ associated with the repulsive interactions affects the holons and is expected to drive a superfluid-Mott transition at a fixed commensurate filling. On the other hand, the fate of the spinons, and specifically their pairing instabilities, is determined by the chiral-exchange interaction. The resulting mean-field Hamiltonian takes the form, $H_{\text{MF}} = H_b(\{\chi\}) + H_f(\{\chi, \Delta, B\})$, where the variational parameters in the matter field sectors are tied to the correlators, $B_{rr'} \equiv \langle b_r^\dagger b_{r'} \rangle$, $\chi_{rr',\sigma}^{\ell\ell'} \equiv \langle f_{r,\ell,\sigma}^\dagger f_{r',\ell',\sigma} \rangle$, and $\Delta_{rr',\sigma\sigma'}^{\ell\ell'} \equiv \langle \varepsilon_{\sigma\sigma'} f_{r,\ell,\sigma} f_{r',\ell',\sigma'} \rangle$, respectively. Clearly, the

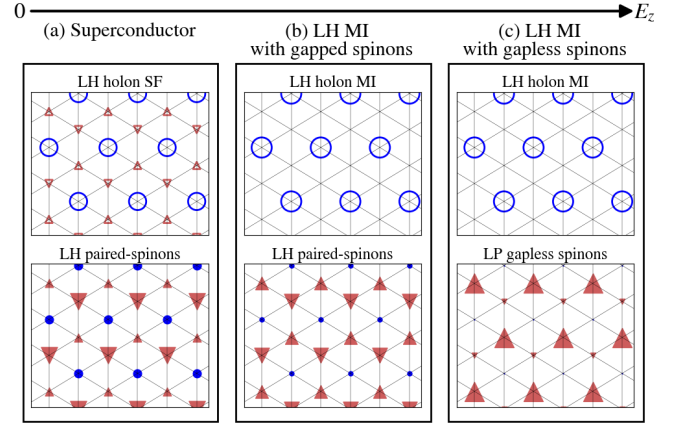


FIG. 2. The evolution of the local occupation for the holons (upper panel) and spinons (lower panel) with increasing displacement-field, (E_z), obtained from the parton mean-field computation for the Hamiltonian in Eq. 1a-3. The empty (\circ, ∇, \triangle) and filled ($\bullet, \blacktriangledown, \blacktriangle$) symbols represent holon and spinon occupations, respectively, on the MM, XM and MX sites. The relative size of the markers is proportional to the respective occupations. LH and LP stand for layer-hybridized and layer-polarized, respectively. (a) For small E_z , both the holons and spinons are LH; the spinons pair leading to an electronic superconductor when the holons are condensed. (b) With increasing E_z , the holons Mott-localize at MM sites and retain their LH character. The spinons are also LH and remain paired, resulting in an electronic MI with charge and spin-gaps, respectively. (c) For larger E_z , we find that the spinons are LP, leading to a significant reduction and eventual loss of pairing.

B -correlator is evaluated with respect to H_b and renormalizes the spinon bandwidth in H_f . Similarly, χ is evaluated with respect to H_f , which arises both from the bare bandwidth and the chiral-exchange term, and renormalizes the boson hoppings in H_b , as well as the spinon hoppings in H_f . Finally, Δ is also evaluated with respect to H_f and drives the pairing of spinons. To deal with H_b , we utilize a 3-site cluster approximation comprising all the three orbitals, within which we impose the global $U(1)$ number conservation. Given that $t_{TH}^{(1)}$ is the dominant hopping, for the preliminary computations that already illustrate key elements of the physics, we consider the equilateral triangles comprising nearest-neighbor orbitals within the clusters.

Results.- Before we describe the outcome of our analysis at a quantitative level, we begin by highlighting some of the key observations at a qualitative level; see Fig. 2. At $E_z = 0$, one of the key bandstructure inputs is the degeneracy tied to MX/XM sites, which is split by $\sim \delta$ from the energy of the MM site. Even at $\nu = 1$, and for the typical values of t_{TH} , t_{HH} , U_H , U_T , V , we find the bosons delocalized across all three orbitals in a superfluid phase, thereby quenching any tendency towards fractionalization. At the same time, the chiral exchange term mediates attraction between the spinons, leading to an *inter-valley* and fully gapped *extended s-wave singlet* paired state. The resulting state is a superconductor. With increasing displacement-field, the energies of the MX/XM sites are no longer degenerate, and split by the field,

and we find an increased tendency towards a Mott transition whereby the holon localizes on the MM sites while the spinons remain delocalized over the MX/XM and MM sites (with unequal average occupation). The Mott transition goes hand in hand with the renormalization of the fermion correlators, χ . With increasing displacement-field, spinons are depleted from the XM sites, and thus the χ that connect the XM and MM/MX sites decrease significantly, driving in part the Mott transition. Importantly, the pattern of charge localization still implies an underlying *layer-hybridized* state. The spinon pairing also survives leading to an insulator with both spin and charge-gap. This is the promised fully-gapped quantum spin liquid insulator. Further increasing the displacement-field, we find that the spinon occupations on the different sublattice sites change rapidly, with $\langle f^\dagger f \rangle_{\text{MM}} \rightarrow 0$. The nature of the chiral exchange interaction (between the MM and MX/XM sites) is such that this automatically also leads to a loss of spinon pairing, without affecting the charge-localization in the Mott insulator. Thus, in one scenario, there is a displacement-field-induced quantum phase transition between a spin-gapped to gapless spin liquid Mott insulator at $\nu = 1$; as long as the holons are localized on the MM sites, both insulators are layer-hybridized.

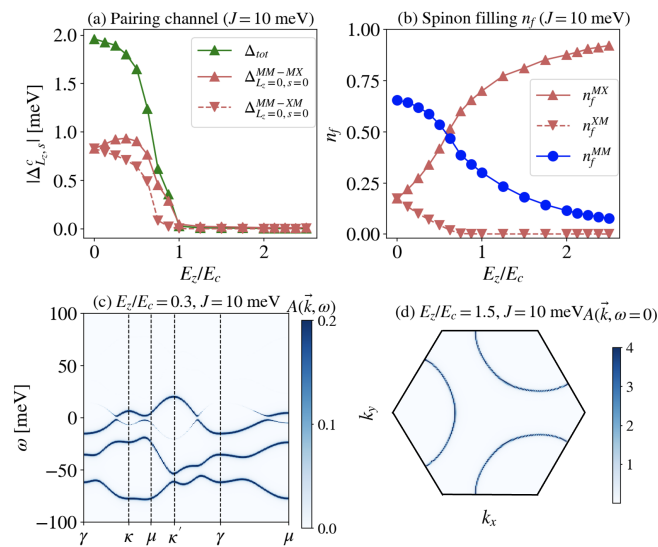


FIG. 3. (a) Spinon pairing-gap Δ_{tot} , obtained from parton mean-field computation as a function of displacement-field, E_z . (b) Evolution of spinon occupation with increasing displacement-field. For $E_z > E_c$, the spinon sector tends to layer polarize. (c) spinon Bogoliubov spectral function $A_f(\mathbf{k}, \omega)$, evaluated at $E_z/E_c = 0.3$ and $J = 10$ meV. A spinon gap ~ 1.5 meV is observed for the half-filled topmost band. (d) Spinon Bogoliubov spectral function $A_f(\mathbf{k}, \omega = 0)$ at $E_z/E_c = 1.5$ and $J = 10$ meV within moiré Brillouin zone. The spinon gap $|\Delta_{\text{tot}}|$ has been fully suppressed and $A(\mathbf{k}, \omega = 0)$ shows the spinon Fermi surface.

Let us now turn to the quantitative results. In Fig. 2 (top-row), we plot the evolution of the holon-densities with increasing displacement-field, obtained from a parton mean-field computation using H_b . As noted above, at small displacement fields, the holons are clearly in a superfluid state

(Fig. 2a), with $\langle b \rangle_\ell \neq 0 \forall \ell$. On the other hand, beyond a critical E_z , numerically we find $\langle b^\dagger b \rangle_{\text{MM}} \approx 1$ and $\langle b \rangle_{\ell \in \text{MM, MX, XM}} \rightarrow 0$. This is the Mott insulating phase (Fig. 2b), which remains layer-hybridized. Eventually, with increasing E , the bosons favor layer-polarization (not shown), where the system effectively becomes a triangular lattice system constructed out of the MX-sites. Simultaneously, it is useful to track the evolution of the spinon-densities with increasing displacement-fields; see Fig. 2 (bottom-row). At small displacement fields, the spinon occupations $\langle f^\dagger f \rangle_\ell \neq 0 \forall \ell$ (Fig. 2a) in a spinon-metallic-like regime, which is unstable to pairing due to the chiral-exchange interaction (Fig. 3). For $J > 0$, attraction is mediated in the inter-valley, spin-singlet channel as noted above. Note that we are technically not including the contributions from the gauge-field fluctuations beyond mean-field theory here, which can suppress the pairing tendency as a result of standard “amperean” effects [44]; we proceed with the assumption that the tendency towards spinon pairing remains prevalent. With increasing displacement-field, the spinon pairing is lost when the spinon-occupation is polarized on to one of the two sublattice sites (MX/XM) of the honeycomb (Fig. 2c).

We have performed a detailed computation of the spinon pairing at the mean-field level; the evolution of the angular-momentum (L_z)-resolved spinon pairing-gap with increasing displacement-field is shown in Fig. 3(a). The angular momentum L_z is defined as the phase winding of the spinon Cooper pairs which live on the three bonds connecting the $T-H$ sites. For arbitrary E_z , only $L_z = 0$ (extended s-wave) and $s = 0$ (spin-singlet) channels develop a finite expectation value. At $E_z = 0$, pairing between MM-MX and MM-XM are on an equal footing due to the presence of inversion symmetry. When $0 < E_z < E_c$, a layer-imbalance develops but the spinon gap $|\Delta_{\text{tot}}|$ remains finite; for $E_z > E_c$, the spinon gap is fully suppressed by E_z , and the spinon sector tends to form a LP spinon-metal (Fig. 3b). These features are reflected in the spinon spectral function, $A_f(\mathbf{k}, \omega)$, in the LH paired (Fig. 3c) and LP unpaired (Fig. 3d) regimes, respectively. Note that we have intentionally refrained from quoting the absolute values of E_z in our analysis, as the values of the layer-polarization susceptibility for both of the matter fields is a priori unknown.

Clearly, the nature of the resulting many-body phase is determined by the combination of the bosonic and fermionic correlators, respectively. When $\langle b \rangle \neq 0$ in the superfluid phase, the resulting state is a superconductor as long as spinon-pairing is present (Fig. 2a). As a function of increasing displacement-field, there can be a tendency towards spontaneously broken C_3 -symmetry [20]. If the holons remain condensed, the resulting state is a nematic superconductor, whereas if the critical field for C_3 -breaking is larger than the Mott transition for the holons, the nematicity onsets only in the gapped spin-liquid insulator. Within our present scenario, when $\langle b \rangle = 0$ in the Mott-insulating phase, for small displacement-fields the ground-state is an electrical insulator with both a charge and spin-gap, respectively. When the spinon pairing is lost, the system transitions into a Mott insulator with a charge-gap but no spin-gap, reminiscent of previous experiments in AA-stacked heterobilayers [45].

Outlook.- The intriguing phenomenology tied to the recently discovered continuous superconductor-to-insulator transition at a fixed commensurate filling in $tWSe_2$ has naturally led us to a scenario where the origin of fermionic pairing (due to spinons) lies in the insulator, and the electrical response (due to holons) is determined purely by the interplay of Hubbard interactions and charge-transfer gap between the different orbitals. Our proposal and preliminary parton mean-field computations already motivates the need for a number of future experiments, which will be crucial for developing deeper theoretical insights into this problem.

First and foremost, the temperature dependence of the magnetic susceptibility in the insulating phase using MCD (at low temperature) will help reveal whether a spin-gap exists along with the charge-gap. This has revealed unparalleled insights in a previous experiment in a Mott-insulator [45]. The above scenario suggests that in the insulator across the transition from the superconductor, the asymptotic low-temperature susceptibility will be exponentially suppressed. It is also plausible, based in part on our computations, that there are two distinct layer-hybridized insulators, separated by a spin-gap closing transition (without any closing of the charge-gap) that can be distinguished at the lowest temperatures based on the MCD data. The ‘kink-like’ feature in the insulating region in the experiment [15] might be indicative of such a transition.

It is worth addressing the possibility of other competing insulating states at $\nu = 1$, that are distinct from our proposal in this manuscript. A possible candidate, given the predominant T -like character of the topmost valence band, is the usual 120-degree ordered local-moment antiferromagnet [37]. However, a direct and continuous transition between such an ordered antiferromagnet and a superconductor at fixed filling is necessarily exotic, without any existing theoretically controlled description. It is also plausible that more exotic in-

solators [46] are at play, but describing a direct continuous transition to the observed superconductor remains a challenge. The experiments nevertheless provide a strong motivation to revisit a careful theoretical study of such quantum phase transitions. Investigating these models using state-of-the-art numerical methods also remains an exciting frontier.

We end by noting that one of the most exciting open questions is related to the nature of the metal-to-metal transition that occurs as a function of filling across the $\nu = 1$ orders at a fixed displacement-field. Approaching from $\nu \rightarrow 1^+$, a renormalized Fermi liquid with an increasing effective mass transitions either into an insulator, or a superconductor in the near vicinity of $\nu = 1$. For $\nu \rightarrow 1^-$, the properties of the metallic state are not entirely clear at present, but there are marked phenomenological differences from a conventional Fermi liquid. Further studies of these metallic phases, incorporating also the effects of disorder, might lead to an improved understanding of the global low-temperature phenomenology in the vicinity of $\nu = 1$ in $tWSe_2$. Within the current scenario, it is worth noting that the superconducting T_c is controlled by the phase-stiffness and not the pairing gap, which can be small both at $\nu = 1$ (e.g. due to disorder effects [47] and suppressed tendency towards pairing [44, 48]) and with doping. Moreover, given the spinonic origin of the pairing, doping away potentially leads to a dramatic suppression of this tendency, when the spinons are prone to confinement. Investigating these effects in more careful detail and utilizing more sophisticated methods remains an interesting open problem.

Acknowledgements.- We are indebted to Zhongdong Han, Kin-Fai Mak, Jie Shan and Yiyu Xia for numerous insightful discussions regarding their experimental results. This work is supported in part by a CAREER grant from the NSF to DC (DMR-2237522) and by a Sloan research fellowship from the Alfred P. Sloan foundation.

-
- [1] Y. Cao, V. Fatemi, S. Fang, K. Watanabe, T. Taniguchi, E. Kaxiras, and P. Jarillo-Herrero, “Unconventional superconductivity in magic-angle graphene superlattices,” *Nature* **556**, 43 (2018).
- [2] M. Yankowitz, S. Chen, H. Polshyn, Y. Zhang, K. Watanabe, T. Taniguchi, D. Graf, A. F. Young, and C. R. Dean, “Tuning superconductivity in twisted bilayer graphene,” *Science* **363**, 1059 (2019).
- [3] X. Lu, P. Stepanov, W. Yang, M. Xie, M. A. Aamir, I. Das, C. Urgell, K. Watanabe, T. Taniguchi, G. Zhang, A. Bachtold, A. H. MacDonald, and D. K. Efetov, “Superconductors, orbital magnets and correlated states in magic-angle bilayer graphene,” *Nature* **574**, 653 (2019).
- [4] H. S. Arora, R. Polski, Y. Zhang, A. Thomson, Y. Choi, H. Kim, Z. Lin, I. Z. Wilson, X. Xu, J.-H. Chu, K. Watanabe, T. Taniguchi, J. Alicea, and S. Nadj-Perge, “Superconductivity in metallic twisted bilayer graphene stabilized by WSe_2 ,” *Nature* **583**, 379 (2020).
- [5] Z. Hao, A. M. Zimmerman, P. Ledwith, E. Khalaf, D. H. Najafabadi, K. Watanabe, T. Taniguchi, A. Vishwanath, and P. Kim, “Electric field-tunable superconductivity in alternating-twist magic-angle trilayer graphene,” *Science* **371**, 1133 (2021).
- [6] M. Oh, K. P. Nuckolls, D. Wong, R. L. Lee, X. Liu, K. Watanabe, T. Taniguchi, and A. Yazdani, “Evidence for unconventional superconductivity in twisted bilayer graphene,” *Nature* **600**, 240 (2021).
- [7] H. Zhou, T. Xie, T. Taniguchi, K. Watanabe, and A. F. Young, “Superconductivity in rhombohedral trilayer graphene,” *Nature* **598**, 434 (2021).
- [8] H. Zhou, L. Holleis, Y. Saito, L. Cohen, W. Huynh, C. L. Patterson, F. Yang, T. Taniguchi, K. Watanabe, and A. F. Young, “Isospin magnetism and spin-polarized superconductivity in bernal bilayer graphene,” *Science* **375**, 774 (2022).
- [9] Y. Zhang, R. Polski, A. Thomson, É. Lantagne-Hurtubise, C. Lewandowski, H. Zhou, K. Watanabe, T. Taniguchi, J. Alicea, and S. Nadj-Perge, “Enhanced superconductivity in spin-orbit proximitized bilayer graphene,” *Nature* **613**, 268 (2023).
- [10] Y. Cao, V. Fatemi, A. Demir, S. Fang, S. L. Tomarken, J. Y. Luo, J. D. Sanchez-Yamagishi, K. Watanabe, T. Taniguchi, E. Kaxiras, R. C. Ashoori, and P. Jarillo-Herrero, “Correlated insulator behaviour at half-filling in magic-angle graphene superlattices,” *Nature* **556**, 80 (2018).
- [11] H. Zhou, T. Xie, A. Ghazaryan, T. Holder, J. R. Ehrets, E. M. Spanton, T. Taniguchi, K. Watanabe, E. Berg, M. Serbyn, and

- A. F. Young, “Half- and quarter-metals in rhombohedral trilayer graphene,” *Nature* **598**, 429 (2021).
- [12] Y. Saito, J. Ge, K. Watanabe, T. Taniguchi, and A. F. Young, “Independent superconductors and correlated insulators in twisted bilayer graphene,” *Nature Physics* **16**, 926 (2020).
- [13] P. Stepanov, I. Das, X. Lu, A. Fahimniya, K. Watanabe, T. Taniguchi, F. H. L. Koppens, J. Lischner, L. Levitov, and D. K. Efetov, “Untying the insulating and superconducting orders in magic-angle graphene,” *Nature* **583**, 375 (2020).
- [14] X. Liu, Z. Wang, K. Watanabe, T. Taniguchi, O. Vafek, and J. Li, “Tuning electron correlation in magic-angle twisted bilayer graphene using coulomb screening,” *Science* **371**, 1261 (2021).
- [15] Y. Xia, Z. Han, K. Watanabe, T. Taniguchi, J. Shan, and K. F. Mak, “Unconventional superconductivity in twisted bilayer WSe₂,” arXiv e-prints, arXiv:2405.14784 (2024), arXiv:2405.14784 [cond-mat.mes-hall].
- [16] L. Wang, E.-M. Shih, A. Ghiotto, L. Xian, D. A. Rhodes, C. Tan, M. Claassen, D. M. Kennes, Y. Bai, B. Kim, K. Watanabe, T. Taniguchi, X. Zhu, J. Hone, A. Rubio, A. N. Pasupathy, and C. R. Dean, “Correlated electronic phases in twisted bilayer transition metal dichalcogenides,” *Nature Materials* **19**, 861 (2020).
- [17] K. Mak, J. Shan, and Z. Han, Private communication.
- [18] A. Kapitulnik, S. A. Kivelson, and B. Spivak, “Colloquium: Anomalous metals: Failed superconductors,” *Rev. Mod. Phys.* **91**, 011002 (2019).
- [19] J. S. Hofmann, E. Berg, and D. Chowdhury, “Superconductivity, charge density wave, and supersolidity in flat bands with a tunable quantum metric,” *Phys. Rev. Lett.* **130**, 226001 (2023).
- [20] C. Schrade and L. Fu, “Nematic, chiral and topological superconductivity in transition metal dichalcogenides,” arXiv e-prints, arXiv:2110.10172 (2021), arXiv:2110.10172 [cond-mat.supr-con].
- [21] Y.-T. Hsu, F. Wu, and S. Das Sarma, “Spin-valley locked instabilities in moiré transition metal dichalcogenides with conventional and higher-order van hove singularities,” *Phys. Rev. B* **104**, 195134 (2021).
- [22] M. Bélanger, J. Fournier, and D. Sénéchal, “Superconductivity in the twisted bilayer transition metal dichalcogenide wse₂: A quantum cluster study,” *Phys. Rev. B* **106**, 235135 (2022).
- [23] M. M. Scherer, D. M. Kennes, and L. Classen, “Chiral superconductivity with enhanced quantized hall responses in moiré transition metal dichalcogenides,” *npj Quantum Materials* **7** (2022), 10.1038/s41535-022-00504-z.
- [24] L. Klebl, A. Fischer, L. Classen, M. M. Scherer, and D. M. Kennes, “Competition of density waves and superconductivity in twisted tungsten diselenide,” *Phys. Rev. Res.* **5**, L012034 (2023).
- [25] Y.-M. Wu, Z. Wu, and H. Yao, “Pair-density-wave and chiral superconductivity in twisted bilayer transition metal dichalcogenides,” *Phys. Rev. Lett.* **130**, 126001 (2023).
- [26] M. Zegrodnik and A. Biborski, “Mixed singlet-triplet superconducting state within the moiré $t-j-u$ model applied to twisted bilayer wse₂,” *Phys. Rev. B* **108**, 064506 (2023).
- [27] W. Akbar, A. Biborski, L. Rademaker, and M. Zegrodnik, “Topological superconductivity with mixed singlet-triplet pairing in moiré transition-metal-dichalcogenide bilayers,” arXiv e-prints, arXiv:2403.05903 (2024), arXiv:2403.05903 [cond-mat.supr-con].
- [28] J. Venderley and E.-A. Kim, “Density matrix renormalization group study of superconductivity in the triangular lattice hubbard model,” *Phys. Rev. B* **100**, 060506 (2019).
- [29] K. Slagle and L. Fu, “Charge transfer excitations, pair density waves, and superconductivity in moiré materials,” *Phys. Rev. B* **102**, 235423 (2020).
- [30] F. Chen and D. N. Sheng, “Singlet, triplet, and pair density wave superconductivity in the doped triangular-lattice moiré system,” *Phys. Rev. B* **108**, L201110 (2023).
- [31] V. Crépel, D. Guerci, J. Cano, J. H. Pixley, and A. Millis, “Topological superconductivity in doped magnetic moiré semiconductors,” *Phys. Rev. Lett.* **131**, 056001 (2023).
- [32] B. Zhou and Y.-H. Zhang, “Chiral and nodal superconductors in the $t-j$ model with valley contrasting flux on a triangular moiré lattice,” *Phys. Rev. B* **108**, 155111 (2023).
- [33] Y.-M. Xie and K. T. Law, “Orbital fulde-ferrell pairing state in moiré ising superconductors,” *Phys. Rev. Lett.* **131**, 016001 (2023).
- [34] C. Broholm, R. J. Cava, S. A. Kivelson, D. G. Nocera, M. R. Norman, and T. Senthil, “Quantum spin liquids,” *Science* **367** (2020).
- [35] P. A. Lee, N. Nagaosa, and X.-G. Wen, “Doping a mott insulator: Physics of high-temperature superconductivity,” *Rev. Mod. Phys.* **78**, 17 (2006).
- [36] T. Senthil and M. P. A. Fisher, “Z₂ gauge theory of electron fractionalization in strongly correlated systems,” *Phys. Rev. B* **62**, 7850 (2000).
- [37] V. Crépel and A. Millis, “Bridging the small and large in twisted transition metal dichalcogenide homobilayers: a tight binding model capturing orbital interference and topology across a wide range of twist angles,” arXiv e-prints, arXiv:2403.15546 (2024), arXiv:2403.15546 [cond-mat.str-el].
- [38] F. Wu, T. Lovorn, E. Tutuc, I. Martin, and A. H. MacDonald, “Topological insulators in twisted transition metal dichalcogenide homobilayers,” *Phys. Rev. Lett.* **122**, 086402 (2019).
- [39] T. Devakul, V. Crépel, Y. Zhang, and L. Fu, “Magic in twisted transition metal dichalcogenide bilayers,” *Nature Communications* **12**, 6730 (2021).
- [40] D. Xiao, G.-B. Liu, W. Feng, X. Xu, and W. Yao, “Coupled spin and valley physics in monolayers of mos₂ and other group-iv dichalcogenides,” *Phys. Rev. Lett.* **108**, 196802 (2012).
- [41] C. Fang, M. J. Gilbert, and B. A. Bernevig, “Bulk topological invariants in noninteracting point group symmetric insulators,” *Phys. Rev. B* **86**, 115112 (2012).
- [42] H. Pan, F. Wu, and S. Das Sarma, “Band topology, hubbard model, heisenberg model, and dzyaloshinskii-moriya interaction in twisted bilayer wse₂,” *Phys. Rev. Res.* **2**, 033087 (2020).
- [43] B. Zhou and Y.-H. Zhang, “Chiral and nodal superconductors in the $t-j$ model with valley contrasting flux on a triangular moiré lattice,” *Phys. Rev. B* **108**, 155111 (2023).
- [44] M. A. Metlitski, D. F. Mross, S. Sachdev, and T. Senthil, “Cooper pairing in non-fermi liquids,” *Phys. Rev. B* **91**, 115111 (2015).
- [45] T. Li, S. Jiang, L. Li, Y. Zhang, K. Kang, J. Zhu, K. Watanabe, T. Taniguchi, D. Chowdhury, L. Fu, *et al.*, “Continuous mott transition in semiconductor moiré superlattices,” *Nature* **597**, 350 (2021).
- [46] A. Szasz, J. Motruk, M. P. Zaletel, and J. E. Moore, “Chiral spin liquid phase of the triangular lattice hubbard model: A density matrix renormalization group study,” *Phys. Rev. X* **10**, 021042 (2020).
- [47] M. P. A. Fisher, P. B. Weichman, G. Grinstein, and D. S. Fisher, “Boson localization and the superfluid-insulator transition,” *Phys. Rev. B* **40**, 546 (1989).
- [48] T. Senthil and P. A. Lee, “Coherence and pairing in a doped mott insulator: Application to the cuprates,” *Phys. Rev. Lett.* **103**, 076402 (2009).